frontiers | Frontiers in Earth Science

TYPE Original Research
PUBLISHED 30 October 2024
DOI 10.3389/feart.2024.1415180

OPEN ACCESS

EDITED BY
Andrea Storto,
National Research Council (CNR), Italy

REVIEWED BY
Yuecong Li,
Hebei Normal University, China
Ronan Connolly,
Center for Environmental Research and Earth Sciences, United States

*CORRESPONDENCE
Sergey A. Gorbarenko,
gorbarenko@poi.dvo.ru

RECEIVED 10 April 2024
ACCEPTED 07 October 2024
PUBLISHED 30 October 2024

CITATION
Gorbarenko SA, Shi X, Liu Y, Bosin AA, Vasilenko YP, Artemova AV, Yanchenko EA, Zou J, Yao Z and Kirichenko IS (2024) Reconstructing Holocene centennial cooling events: synthesized temperature changes, chronology, and forcing in the Northern Hemisphere.
Front. Earth Sci. 12:1415180.
doi: 10.3389/feart.2024.1415180

Reconstructing Holocene centennial cooling events: synthesized temperature changes, chronology, and forcing in the Northern Hemisphere

Sergey A. Gorbarenko[1]*, Xuefa Shi[2,3], Yanguang Liu[2,3,4], Aleksandr A. Bosin[1], Yuriy P. Vasilenko[1], Antonina V. Artemova[1], Elena A. Yanchenko[1], Jianjun Zou[2,3], Zhengquan Yao[2,3] and Ivan S. Kirichenko[5]

[1]V.I. Il'ichev Pacific Oceanological Institute, Far East Branch of the Russian Academy of Sciences, Vladivostok, Russia, [2]Key Laboratory of Marine Geology and Metallogeny, First Institute of Oceanography, Ministry of Natural Resources, Qingdao, China, [3]Laboratory for Marine Geology, Qingdao Marine Science and Technology Center, Qingdao, China, [4]College of Ocean Science and Engineering, Shandong University of Science and Technology, Qingdao, China, [5]Geology and Mineralogy Institute, Siberian Branch of the Russian Academy of Sciences, Novosibirsk, Russia

Numerous studies, spanning experimental, instrumental, historical, and modeled approaches, have delved into understanding climate change across the Holocene era and millennial-scale occurrences. However, the chronology and causes of centennial-scale climate events during the Holocene remain controversial. In this study, we overviewed 10 of the best-resolved and most accurately dated records detailing climate change in the Northern Hemisphere (NH) over the Holocene, obtained from different proxies across different climatic zones, and constructed a stack of temperature changes in the NH. Based on the constructed stack, we identified and categorized 15 notable Holocene centennial cooling events (HCCEs) in the NH (period with temperature decreases). To test the chronological validity of the constructed HCCEs, we compared them with the most accurately dated and highly resolved climate records during the last 3 kyr, which have been extensively investigated by the scientific community. Based on the close alignment of the outlined HCCEs with temperature records, we suggest that other HCCEs also match centennial climate cooling events over the last 10 kyr. To understand the origins of the established HCCEs, we compared them with potential climate influencing factors: total solar irradiance (TSI), explosive volcanic activity, Atlantic meridional overturning circulation (AMOC)-limited slowdowns, Intertropical Convergence Zone (ITCZ) fluctuations, and El Niño/Southern Oscillation (ENSO variability. Early Holocene HCCE 5, terminated by a prominent 8.2-ka cold event, was likely driven by the superposition of the AMOC limited slowdown, TSI minimum, and volcanic activity. The Holocene Thermal Maximum (HTM) happened between HCCEs 5 and 4a and was interrupted by HCCE 4c and 4b, coeval, with a significant southward shift of the ITCZ, likely related to cooling in the tropical zone. However, the sequence of HCCEs 3b, 3a, and 2b (over 4.53–3.42 BP), accompanied by small changes in the TSI, was likely forced by an increase in

ENSO variability, leading to remarkable changes in the tropical processes and a southward shift of the ITCZ, coeval with the collapse of the Chinese Neolithic cultures and onset of the Holocene Neoglacial. Subsequent HCCEs 2a–0a were likely forced by the TSI minimum combined with the influence of ENSO and volcanism over the last 2 ka.

KEYWORDS

climate cooling, Holocene, centennial scale, climate forcings, Northern Hemisphere

1 Introduction

The warm climate of the present interglacial period, which began 11.7 kyr BP after the cold event of the Younger Dryas (Alley et al., 1993), contributed to the intensive development of human society. Although the Holocene climate was not stable, the sequence of sharp and strong climate changes, such as the Dansgaard–Oeschger cycles, which occurred during the last glaciation (Dansgaard et al., 1993), did not reoccur.

Multidecade, centennial, and millennial climate changes have brought significant environmental transformations across various regions (Denton and Karlén, 1973; Stager et al., 1997). Some of these shifts led to catastrophic disruptions of human civilizations, such as the collapses of well-documented Chinese Neolithic cultures and the Eastern Mediterranean Late Bronze Age (Dark Age) at approximately 4 kyr BP and 3.15–2.95 kyr BP, respectively (Wu and Liu, 2004; Sun et al., 2019; Kaniewski et al., 2010; Margaritelli et al., 2020). Therefore, high-resolution reconstruction of both local and global shifts in temperature and precipitation patterns across the Holocene period is paramount for understanding millennial–centennial natural climate changes over the Holocene and the external and internal origins behind them. Consequently, the scientific community has undertaken numerous experimental, theoretical, and modeling explorations into Holocene climate dynamics, with a notable surge in research activity (Bailey et al., 2018; Brooks et al., 2015; Döring and Leuenberger, 2022; Kaufman and Broadman, 2023; Kobashi et al., 2017; Mann et al., 2009; Mayewski et al., 2004; Moy et al., 2002; Marcott et al., 2013; Nazarova et al., 2021; Razjigaeva et al., 2022; Solomina et al., 2015; Sun et al., 2019; Wang et al., 2005; 2008; Wanner et al., 2011; 2015). The findings provided important insights into regional temperature and precipitation fluctuations throughout the Holocene through multiproxy investigations encompassing lakes, peatlands, tree rings, continental sediments in the Eurasian and American continents, and ice and marine sediment cores (Briffa et al., 2001; Bond et al., 2001; Brooks et al., 2015; deMenocal et al., 2000; Esper et al., 2002; Harding et al., 2023; Mann et al., 2008; Tarasov et al., 2019; Herzschuh et al., 2023).

Several generalizations of the climate and temperature changes throughout the Holocene have been attempted (Bond et al., 2001; Mann et al., 2008; Wanner et al., 2011; 2015; Marcott et al., 2013; Kaufman and Broadman, 2023). Consequently, the most important climatic events of the Holocene have been established: the cold event 8.2 kyr BP, the Holocene Thermal Maximum (HTM), the Mid-Holocene Optimum (MHO), the Roman Warm Period (RWP), the Medieval Warm Period (MWP), and the Little Ice Age (LIA) (Bond et al., 2001; Mann et al., 2009; Brooks et al., 2015; Wanner et al., 2015; Kobashi et al., 2017; Margaritelli et al., 2020). Bond et al. (2001) found several cycles of sea ice intensification in the North Atlantic sediments forced by climate cooling over the Holocene and related them to the persistent influence of solar irradiation on the climate. Marcott et al. (2013) compiled 73 quantitative marine–margin temperature records, reconstructed regional and global temperature anomalies for the past 11,300 years, and confirmed a pattern of early Holocene (10–5 ka) warmth, followed by 0.7°C of cooling through the middle to late Holocene with an averaged time resolution of approximately 120 years. Mann et al. (2008) presented an expanded set of proxy data for decadal to centennial climate change, updated instrumental data, and reconstructed new land and land–ocean climate records over the last 1.8 kyr through complementary methods and model simulation. Wanner et al. (2011) reconstructed six cold events throughout the Holocene based on published evidence of temperature and precipitation shifts and glacier advances documented in various natural repositories; these events were correlated to Bond-like cycles.

In contrast to proxy-reconstructed global temperature records, which mostly show climate cooling in the late Holocene, Liu et al. (2014), based on three coupled ocean–atmosphere models, demonstrated a gradual warming over the Holocene. This highlights the discrepancies between paleoclimate records and model simulations, the so-called "Holocene Temperature Conundrum." Marsicek et al. (2018) re-analyzed pollen evidence from 642 sites across North America and Europe and inferred that long-term warming, instead of cooling, was defined in the Holocene until approximately 2 ka ago and concluded that long-term cooling over the Northern mid–high latitudes was limited to the North Atlantic. Recently, Herzschuh et al. (2023) overviewed 1,908 pollen records in the Northern Hemisphere (NH) extra-tropics and inferred pollen-based reconstructions of latitudinal and regional mean annual temperature, mean July temperature, and annual precipitation for the NH over the last 11 ka. The authors identified strong latitudinal patterns in the temperature trends and differences between subcontinents. If the circum-Atlantic regions in Europe and eastern North America show a pronounced mid-HTM, western North America shows only weak changes, while Asia mostly shows a continuous Holocene temperature increase. However, despite the significant increase in the number of proxy-based reconstructions over the past decades, there is still a lack of synthesis of the dated main modes of the Holocene climate and temperature variability and forcings behind them.

In this study, we focused on the synthesis of the marine–coastal NH temperature stack based on several newly published, well-dated climate change records over the last 10 ka with extra high

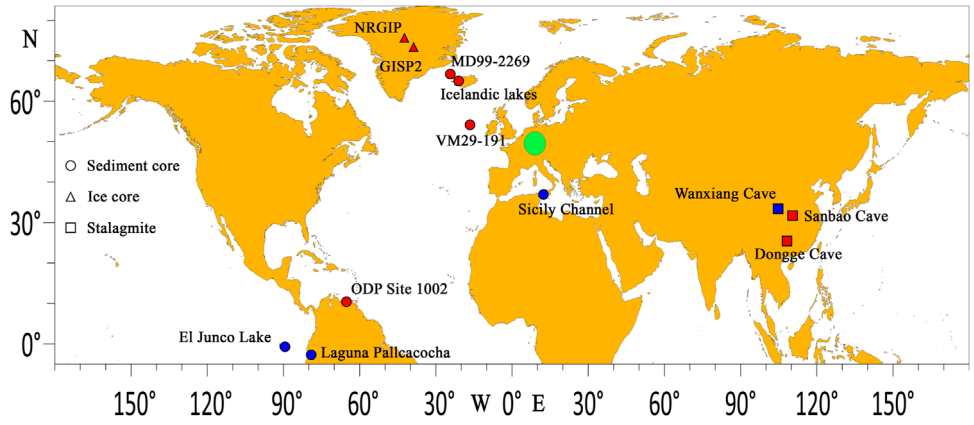

FIGURE 1
Site locations used for temperature stack construction (Bond et al., 2001; Haug et al., 2001; Wang et al., 2005; Moros et al., 2006; Dong et al., 2010; Geirsdóttir et al., 2013; Rasmussen et al., 2014; Kobashi et al., 2017; Döring and Leuenberger, 2022) (red symbols) and for European temperature reconstructions based on tree rings (Büntgen et al., 2006; 2011) (green circle) and other mentioned sites (blue symbols).

time resolution, which mostly responded to mid–high-latitude NH temperature changes.

An important input into the very high temporal with excellent chronology reconstruction of the high-latitude NH temperature changes provides marine–margin compiled temperature records for 30–90 °N (Marcott et al., 2013), the Greenland ice core $\delta^{18}O$ record (Rasmussen et al., 2014), and two new Greenland Summit temperature reconstructions using nitrogen and argon isotopes of trapped air within GISP2 ice core bubbles (Kobashi et al., 2017; Döring and Leuenberger, 2022). Isotopic geochemical studies of stalagmites from caves in China and other regions have made invaluable contributions to high-resolution and well-dated research on the Holocene climate (Neff et al., 2001; Wang et al., 2005; Ma et al., 2008; Dong et al., 2010; Li et al., 2019). The activity of the East Asia Summer Monsoon, inferred from the stalagmite $\delta^{18}O$ records from the East China caves (Sanbao and Dongge), was mostly determined by regional precipitation variability and significantly forced by temperature changes in the tropical Pacific. The meridional migration of the northern boundary of the Intertropical Convergence Zone (ITCZ), determined in the Ti content of ODP site 1002 (Haug et al., 2001), also largely depends on the NH temperature changes. Records of ice-rafted debris (IRD) from the North Atlantic sediments (Bond et al., 2001; Moros et al., 2006) are obtained under strong variability of northern mid–high-latitude temperature changes. The records of multi-proxy physical and organic matter proxies of the lacustrine sediments in Iceland (Geirsdóttir et al., 2013) are also mostly forced by the temperature variability of the North Atlantic. In the last decades, the tight in-phase teleconnection of the millennial climate changes between the North Atlantic and the North Pacific by atmosphere circulation was established by numerous paleo investigations on the glacial and deglacial periods (Seki et al., 2004; 2009; Gorbarenko et al., 2007; 2017; Max et al., 2012; 2014; Riethdorf et al., 2013b; 2013a; Corrick et al., 2020; Duan et al., 2023). Therefore, although the mid–high-latitude NH temperature records (Figure 1) were obtained mainly for the North Atlantic, we suggest that these centennial events are responsible for the marine–coastal temperature changes in the mid–high latitudes of the NH over the Holocene.

Based on the synthesized marine–coastal temperature stack, we outlined the sequence of the most significant Holocene centennial cooling events (HCCEs) in the NH over the last 10 ka and investigated the potential external and internal forcing mechanisms that had affected the formation of these HCCEs detailed in our robust chronology. Although previous research had established linkages between Holocene climate shifts and solar activity (Bond et al., 2001; Wang et al., 2005), the variability in Holocene climate is influenced by an array of additional forcing factors beyond solar activity (Steinhilber et al., 2012).

2 Materials and methods

We synthesized highly resolved Holocene temperature changes in the NH by overviewing the 10 most accurately dated and highly resolved climate change records spanning the past 10 kyr. The main criteria for the selection of used climate records are as follows: detailed and robust age models based on the AMS ^{14}C or ^{230}Th dating, well-established tephrochronology, sediment physical proxy like paleomagnetic secular variation and layer counting; extremely high temporal resolution of records up to several years; marine/near coastal location of selected records at different parts of the North Hemisphere; longer and more discontinuous records throughout the Holocene; and a set of selected records that include several types of independent proxies (S1). These records are drawn from distinct locations across the NH, each falling within different climatic zones (Figure 1).

The selected records encompass $\delta^{18}O$ data from the NGRIP Greenland ice core (Rasmussen et al., 2014), two Greenland Summit temperature reconstructions using nitrogen and argon isotopes of trapped air within GISP2 ice core bubbles (Kobashi et al., 2017; Döring and Leuenberger, 2022), a zonal temperature stack for latitudes 30°–60° in the NH (Marcott et al., 2013), IRD accumulation data from sediment cores VM29–191 and MD99–2269 in the

North Atlantic (Bond et al., 2001; Moros et al., 2006), Ti content in sediments from ODP site 1002 in the northern Cariaco Basin (Haug et al., 2001), records of East Asian summer monsoon (EASM) changes from $\delta^{18}O$ stalagmites in Chinese Dongge (Wang et al., 2005) and Sanbao (Dong et al., 2010) caves, and composite climatic records from Icelandic lakes (Geirsdóttir et al., 2013) (Figure 2). A brief overview of the used NH climate records with details of individual temporal resolution and accuracy of chronology over the Holocene is presented in Supplementary Material.

Based on a careful estimation of the 10 generalized best-dated records with the highest resolution, we excluded the famous IRD record obtained by Bond et al. (2001) because of the lower time resolution of the studied VM29–191 core, with a length of 2 m. We also excluded the Greenland temperature change estimation obtained by Kobashi et al. (2017) due to errors in temperature calculation, according to Döring and Leuenberger (2022) (Figures 2D,H).

For the construction of the NH temperature stack, we used the mentioned climate records on their original age model, and the age of each record was recalculated to a uniform age scale, where 1950 CE was taken as 0 (ka BP). While retaining the original age models for the selected best-dated climate records with the highest temporal resolution, we acknowledge some discrepancies in the timing of abrupt climate shifts due to age model imperfections and potential short-term sediment accumulation distortions in some individual cores. Thus, an age correction was applied to the lacustrine record obtained by Geirsdóttir et al. (2013), notably for the abrupt minima at 2.9 kyr BP, spanning 3.2–2.5 kyr BP, to align it with the well-dated Homeric Grand Solar Minimum (HGSM) (Goslar, 2003; Usoskin et al., 2007; Steinhilber et al., 2012) (Figure 2F). Given the evidence highlighting the significant impact of the HGSM on the abrupt climate decline in the NH (Wang et al., 2005; Steinhilber et al., 2012; Harding et al., 2023), we adjusted the Geirsdóttir stack minima by approximately 150 years, placing it within the HGSM at an age of 2.715 kyr BP (Usoskin et al., 2007). Furthermore, we introduced some corrections to the titanium content record in the sediments of ODP site 1002 from the study by Haug et al. (2001). When comparing the centennial–millennial trends in this record with those of EASM and other accepted records (Figure 2J), we observed a close consistency in trends throughout the Holocene, except for the interval spanning 3.2–2.5 kyr BP. The record obtained by Haug et al. (2001) over this period shows unusually strong zigzag changes, likely induced by sediment perturbation. To address the period of 3.2–2.5 kyr BP, we excluded data from the records obtained by Haug et al. (2001) and calculated the Holocene NH temperature stack for this specific period using seven other records. The gap in the SB43 record was filled with coeval data from SB10 while compiling the Sanbao composite record (Dong et al., 2010) (Figure 2C). The age model of the sediment core MD99–2269 (Moros et al., 2006) was adjusted following Stoner et al. (2007). Chronological uncertainties in the paleoclimate time series used for synthesizing the temperature stack are typically 1%–1.5% of the absolute age, for example, between 100 and 150 years for a 10,000-year-old sample.

To average the highly resolved and best-dated climate records used in this study, we constructed a marine–coastal NH temperature stack over the Holocene at the centennial scale. All records were linearly interpolated to 10-year resolution and detrended and normalized by subtracting the mean value and dividing by the standard deviation. The marine–coastal NH temperature stack was smoothed using a 150-year moving average window. The monsoon stack shown in Figure 4 was calculated in the same way using two EASM records (Wang et al., 2005; Dong et al., 2010).

Based on a constructed temperature stack, instead of typical cold climate events over the Holocene (Wanner et al., 2011), we detected the HCCEs that outline the sequence of periods with significantly decreased temperatures in the marine–coastal areas of the NH. Therefore, HCCE boundaries may be refined by the negative rate of the temperature stack changes over the Holocene (negative first derivative of the stack, d(stack)/dt, dt = 30 years) (Figure 2).

3 Results

3.1 Synthesizing the multi-decadal–centennial record of Holocene temperature changes and HCCEs in the NH

The resulting temperature stack derived from 8 meticulously dated and highly resolved climate records presents the sequence of 15 larger and more prolonged centennial HCCEs labeled as 0a, 0b, 1a, 1b, 1c, 1d, 2a, 2b, 3a, 3b, 4a, 4b, 4c, 5, and 6, over the last 10 kyr, with numeration following Bond cycles (Bond et al., 2001) (Figure 2, Table 1). We should note that these 15 HCCEs derived from our new temperature stack might differ slightly from the equivalent events described in other studies. There are also other smaller and less prolonged cooling events suggested by our constructed temperature stack (Figure 2). However, the primary focus of this paper is the more remarkable and long-lasting changes in NH temperature over the Holocene. In this study, we concentrate on the natural Holocene climate changes and exclude the anthropogenic influence on climate, actively discussed by the scientific community. According to data presented by NOAA Climate.gov (https://www.climate.gov/news-features/understanding-climate/climate-change-atmospheric-carbon-dioxide), CO_2 emissions into the atmosphere started nearly since 1850 yr CE, and therefore, CO_2 content in the atmosphere began to slowly increase after 1850 CE. Therefore, we suggest that the constructed temperature stack ends at nearly 1850 years of Common Era (100 years BP).

4 Discussion

4.1 Comparing HCCEs with available climate records over the last 3,000 years

A comparison of the constructed temperature stack and HCCEs with several highly resolved and well-dated temperature and climate records of the NH and variability in the main centers of atmospheric circulation in the NH over the best-investigated last 3,000 years is crucial for the temporal verification of the reconstructed HCCEs over the last 10 ka (Figure 3).

The HCCE 2a (2.96–2.70 kyr BP) is marked by significant temperature decreases in the Mediterranean Sea surface waters (Margaritelli et al., 2020) and climate records from the Hvítárvatn

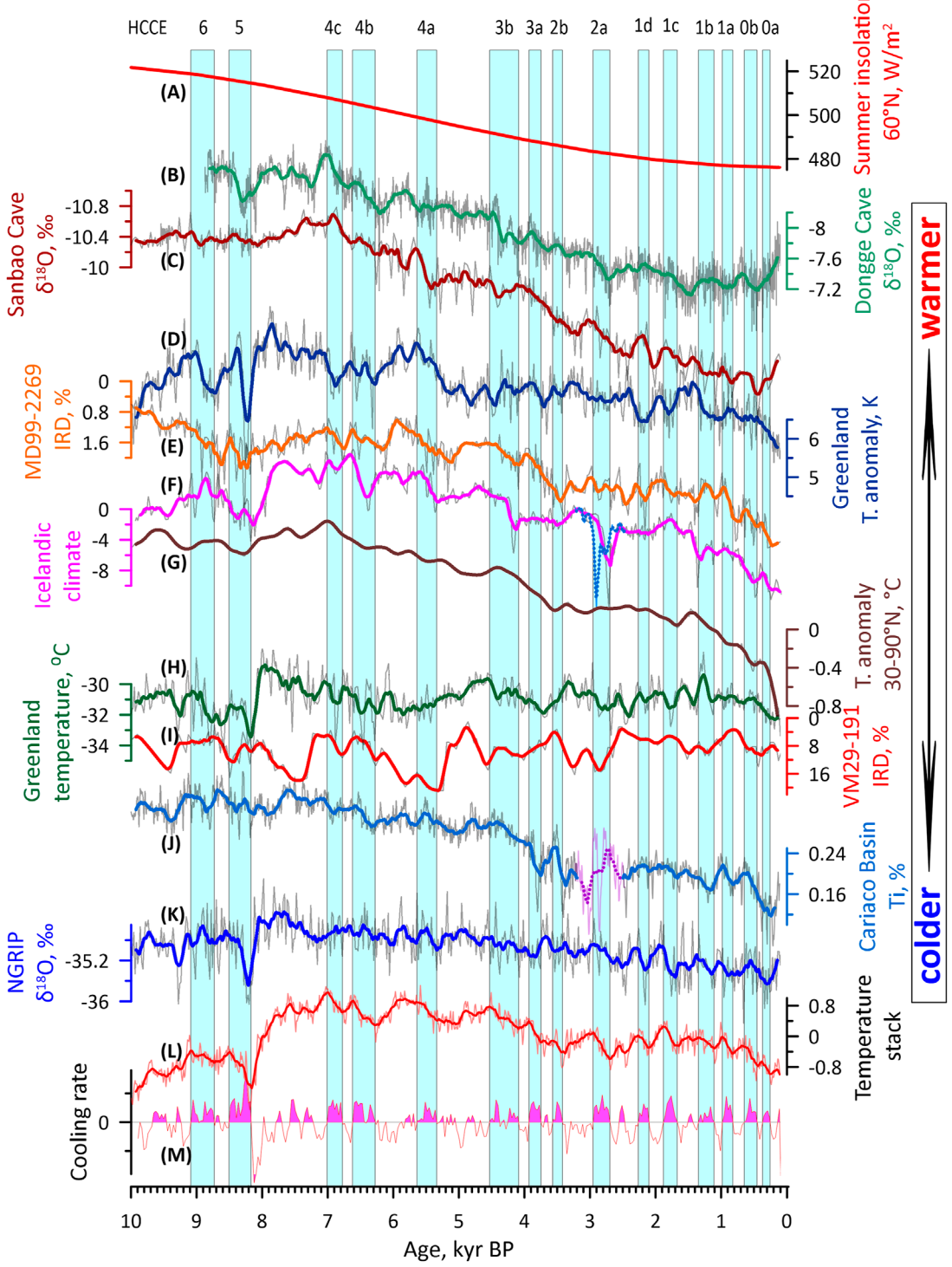

FIGURE 2
Published records used for stack construction, synthesis of the marine–coastal NH temperature stack, and cooling rate and outlined HCCEs. **(A)** Summer solar insolation at 60°N (Berger, 1978); **(B)** oxygen isotopic records of stalagmites from the Dongge Cave (Wang et al., 2005) and **(C)** Sanbao Cave (Dong et al., 2010); **(D)** and **(H)** Greenland Summit temperatures records obtained by Döring and Leuenberger (2022) and Kobashi et al. (2017), respectively; **(E)** and **(I)** IRD records in the North Atlantic sediment cores MD99–2269 (Moros et al., 2006) and VM29–191 (Bond et al., 2001), respectively; **(F)** composite climatic record from Icelandic lakes (Geirsdóttir et al., 2013); **(G)** zonal temperature stack for 30°–60° latitudes of the NH (Marcott et al., 2013); **(J)** titanium content in sediments of ODP site 1002 from the northern Cariaco Basin (Haug et al., 2001); **(K)** $\delta^{18}O$ of Greenland ice core NGRIP (Rasmussen et al., 2014); **(L)** synthesized temperature stack; and **(M)** rate of temperature stack changes (cooling rate). Top records **(B–K)** are related to warming, while bottom records are related to cooling.

TABLE 1 Sequence of HCCEs and their chronology in the Northern Hemisphere, outlined from synthesized temperature stack.

HCCE	Chronology, kyr BP (before 1950 yr CE)
0a	0.37–0.26
0b	0.65–0.46
1a	0.98–0.83
1b	1.35–1.12
1c	1.89–1.68
1d	2.27–2.11
2a	2.96–2.70
2b	3.58–3.42
3a	3.94–3.75
3b	4.53–4.09
4a	5.64–5.34
4b	6.62–6.28
4c	7.02–6.78
5	8.51–8.18
6	9.09–8.74

Lake of Iceland (Geirsdóttir et al., 2013) (Figures 3A, B). The action of the main NH atmospheric circulation centers and oscillations—Siberian High (SH)/North Westerly (NW) and North Atlantic Oscillation (NAO)—also contributes to the cooling of the NH (Figures 3F, G).

HCCE 1d (2.27–2.11 kyr BP) had occurred coeval with insignificant decreases in European temperature, cooling in the Hvítárvatn Lake (Geirsdóttir et al., 2013), and low temperature in the Mediterranean Sea surface waters (Margaritelli et al., 2020) (Figures 3A–C). A certain amount of weakening in the EASM activity (Figures 2B, C) and a shift to the negative phase of NAO were observed over the middle–late phase of HCCE 1d, consistent with the coeval temperature stack decrease in the NH (Figures 3F, I).

HCCE 1c (1.89–1.68 kyr BP) occurred approximately 80 years after the onset of the RWP, which was marked by a significant increase in temperature in European records (Büntgen et al., 2011) and extra-tropical NH (Ljungqvist, 2010) (Figures 3C, E). During HCCE 1c, a significant decrease in the NH extra-tropical temperature anomaly and a slight decrease in European temperature and atmospheric SH/NW oscillation (Figures 3C, E, G) occurred. The warmer part of the RWP likely occurred after HCCE 1c in its later phase, according to the Mediterranean water temperature and positive NAO (Figures 3A, F).

HCCE 1b (1.35–1.12 kyr BP) occurred coeval with a decrease in the temperature of the Mediterranean Sea (Margaritelli et al., 2020) and a significant weakening of the EASM activity recorded in the Wanxiang Cave (Zhang et al., 2008) related to NH cooling (Figures 3A, H). Other temperature curves and the NAO index do not contradict such changes (Figures 3A–F).

HCCE 1a (0.98–0.83 kyr BP) was also well defined by a temperature decrease in the European Alps record obtained by Büntgen et al. (2006), land–ocean reconstructions conducted by Mann et al. (2008), and extra-tropical NH observations obtained by Ljungqvist (2010) (Figures 3D, E). Weakening of the EASM, recorded in the Chinese cave Wanxiang (Zhang et al., 2008), also confirmed climate cooling during HCCE 1a (Figure 3H). HCCE 1a occurred after the onset of the MWP, which was outlined by a large increase in temperature of the European, NH land–ocean, and NH extra-tropical records and EASM activity in the Wanxiang Cave, with a lag of nearly 50 years (Figures 3C–E, H).

HCCE 0b (0.65–0.46 kyr BP) had occurred nearly 70 years earlier than the onset of the LIA (Mann et al., 2009), which was well recorded by the temperature decrease in Germany, the NH land–ocean record obtained by Mann et al. (2008), and extra-tropical NH records obtained by Ljungqvist (2010) (Figures 3C–E). The timing of the LIA was also consistent with cooling in atmospheric circulation (shift to negative NAO and enhancement of SH/NW) (Figures 3F, G). The onset of HCCE 0b was coeval with cooling in the European Alps temperature records (Büntgen et al., 2006; 2011), the extra-tropical temperature curve of the NH (Ljungqvist, 2010), and the EASM activity recorded in the Chinese Wanxiang cave (Zhang et al., 2008) (Figures 3C, E, H). Short-term warming between HCCEs 0b and 0a (0.46–0.37 ka BP) occurred coeval with an abrupt increase in European temperature (Büntgen et al., 2006), the NH temperature record obtained by Ljungqvist (2010), and the Iceland climate curve (Geirsdóttir et al., 2013) (Figures 3B, C, E). This short-term warming within the LIA was also accompanied by some amelioration in atmospheric circulation according to a shift to positive NAO (Figure 3F, F). NH temperature decrease, outlined by less pronounced HCCE 0a (0.37–0.26 ka BP), occurred coeval with most records of the temperature changes and cooling in the NH atmosphere circulation patterns (NAO and SH/NW) (Figures 3A–C, E–G).

The nearly close alignment of outlined HCCEs 2a, 1d, 1c, 1b, 1a, 0b, and 0a with most of the temperature reconstructions in NH, as well as correspondence with the variability in the main atmospheric circulation centers (NAO, SH/NW, and EASM) over the last 3 kyr (Figure 3), suggests that other HCCEs match centennial cooling over the last 10 kyr in the NH. HCCEs 1c and 1a clarify the decadal to centennial-scale climate fluctuations during the warmer periods of the Late Holocene, specifically the RWP and MWP, respectively.

4.2 Possible forcing mechanisms of the HCCEs

Multiple potential forcings have been deliberated within the scientific community as drivers behind Holocene centennial climate cooling linked to the outlined HCCEs, including variability in the total solar irradiance (TSI) (Bond et al., 2001; Wang et al., 2005; Solomon et al., 2007; Steinhilber et al., 2012; Egorova et al., 2018), large volcanic eruptions (Zhong et al., 2011; Sigl et al., 2015; Kobashi et al., 2017; Sigl et al., 2022), the episodic increases in

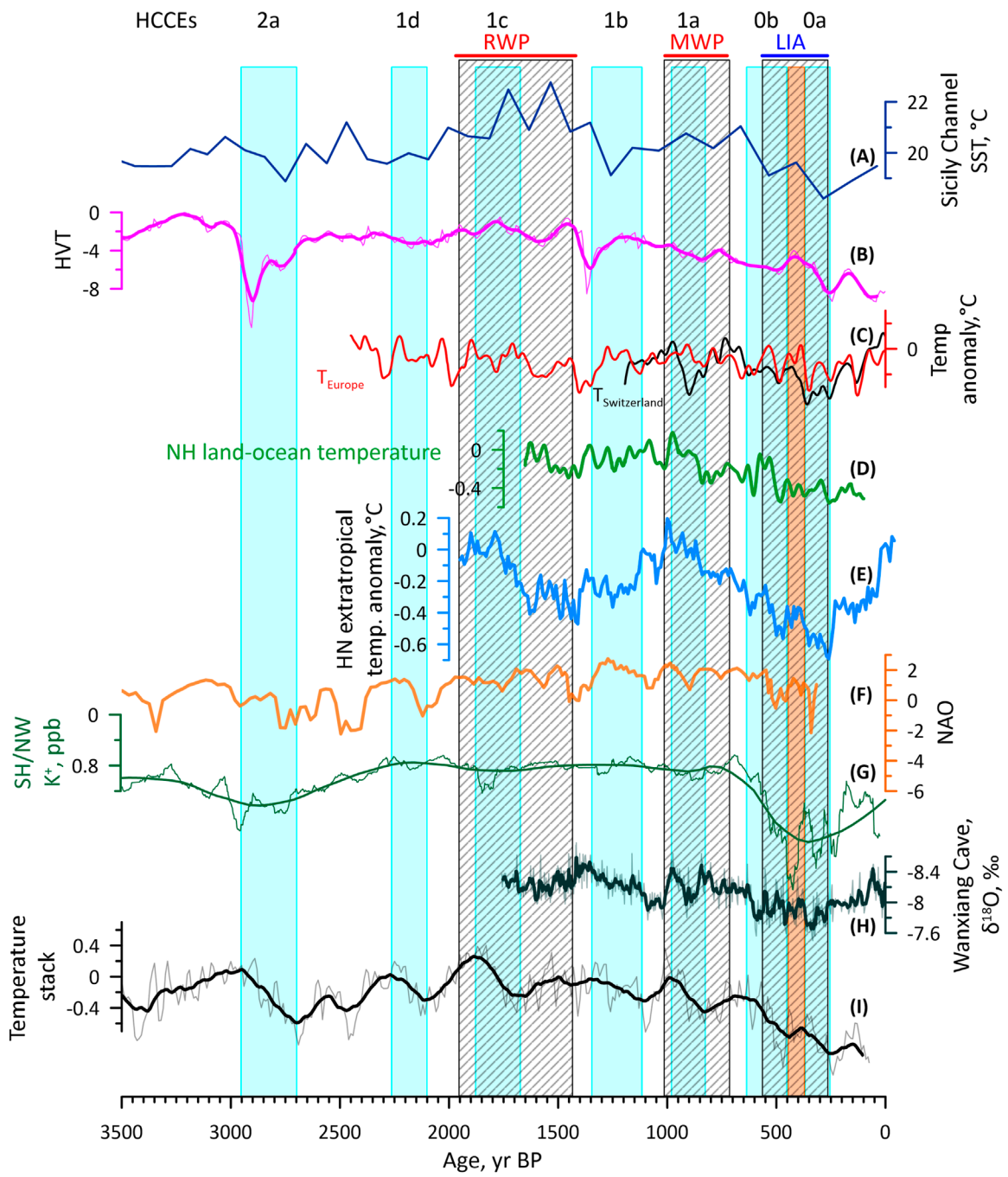

FIGURE 3
Comparison of the synthesized stack and HCCEs with available temperature records and variability of the main centers of the NH atmosphere circulation over the last 3,000 years: **(A)** Mediterranean Sea surface water temperature (Margaritelli et al., 2020); **(B)** composite record of the Hvítárvatn Lake from Iceland (Geirsdóttir et al., 2013); **(C)** Central European temperature records (Büntgen et al., 2006; 2011); **(D)** NH land–ocean surface temperature record (Mann et al., 2008); **(E)** temperature variability in the extra-tropical NH (Ljungqvist, 2010); **(F)** NAO variability (Olsen et al., 2012); **(G)** SH/NW record (Mayewski et al., 2004); **(H)** EASM activity from oxygen isotopic records of the China Wanxiang Cave (Zhang et al., 2008); and **(I)** synthesized stack. HCCEs are indicated with blue bars. The RWP, MWP, and LIA are indicated with hatched bars. The yellow bar shows short-term warming between HCCEs 0a and 0b.

the flux of freshwater to the North Atlantic caused by accelerated melting of the Laurentide ice sheets (Mauritzen and Häkkinen, 1997; Clark et al., 2001; Buckley and Marshall, 2016), El Niño/Southern Oscillation (ENSO) variability (Bjerknes, 1969; Wang et al., 2001; Cane, 2005), and meridional migration of the ITCZ (Haug et al., 2001; Schneider et al., 2014). These climate forcing mechanisms, in turn, influenced shifts in atmospheric circulation centers and their interactions within the ocean–atmosphere system, thereby resulting in changes in the climate and environmental conditions of the NH.

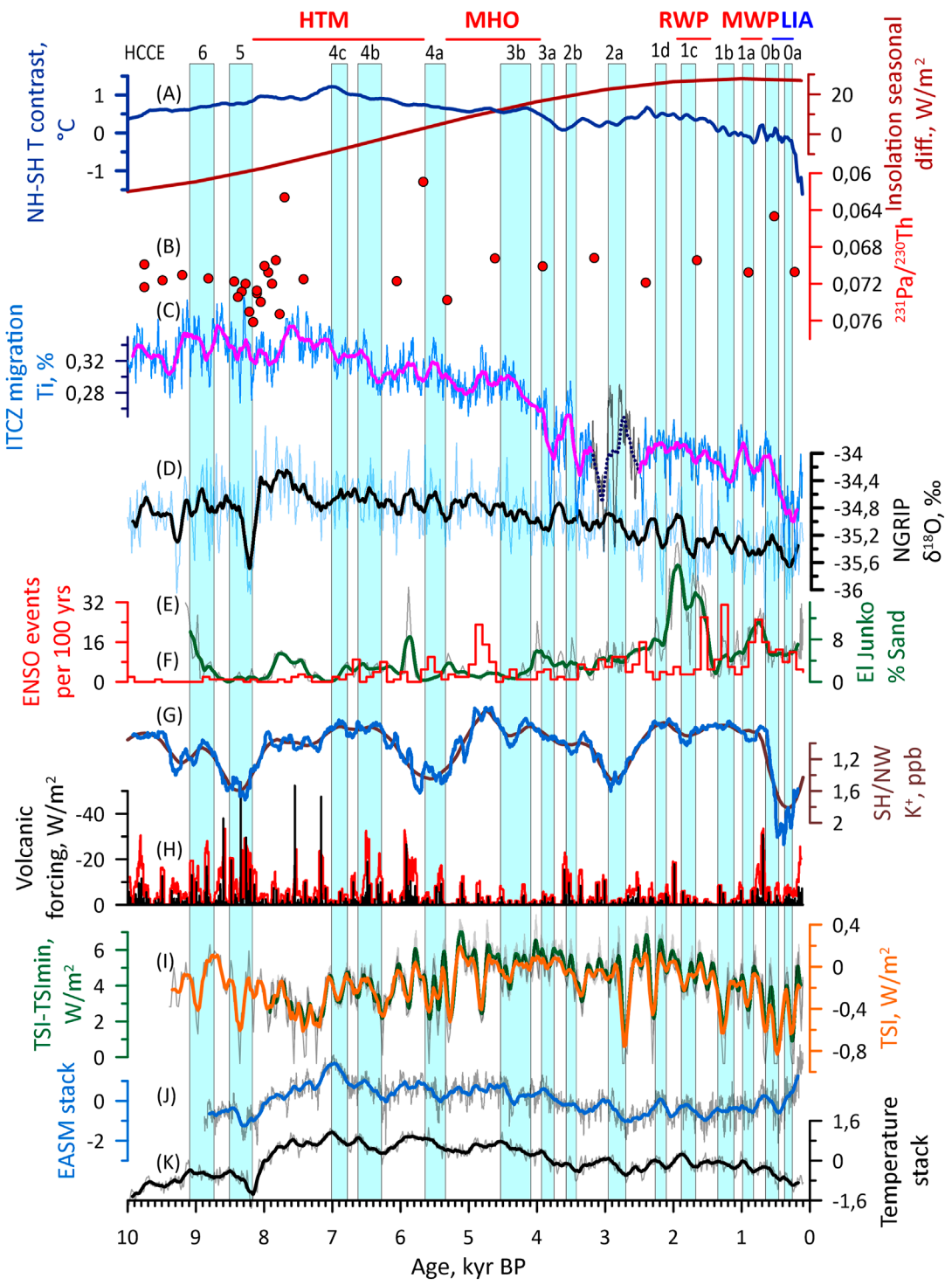

FIGURE 4
Comparison of outlined HCCEs with potential climate forcings and related global climate changes. **(A)** Temperature difference between the Northern and Southern Hemispheres (Marcott et al., 2013) for poleward areas of 30°N and 30°S (blue line), mid-month insolation difference between December and June in the tropical latitudes (Berger et al., 1993) (ruby red line); **(B)** AMOC variability record (Hoffmann et al., 2018); **(C)** titanium content in sediments of ODP site 1002 from the northern Cariaco Basin (Haug et al., 2001); **(D)** $\delta^{18}O$ of Greenland ice core NGRIP (Rasmussen et al., 2014); **(E)** and **(F)** ENSO variability records obtained by Conroy et al. (2008) and Moy et al. (2002), respectively; **(G)** SH/NW record (Mayewski et al., 2004); **(H)** volcanic forcing (Kobashi et al., 2017); **(I)** TSI according to Steinhilber et al. (2012) and Egorova et al. (2018) (orange and green lines, respectively); **(J)** EASM stack (Wang et al., 2005; Dong et al., 2010); and **(K)** synthesized temperature stack. HCCEs are shown by light blue vertical bars with numbering at the top. HTM and MHO are shown by red lines at the top. HCCEs are depicted similar to Figures 2, 3.

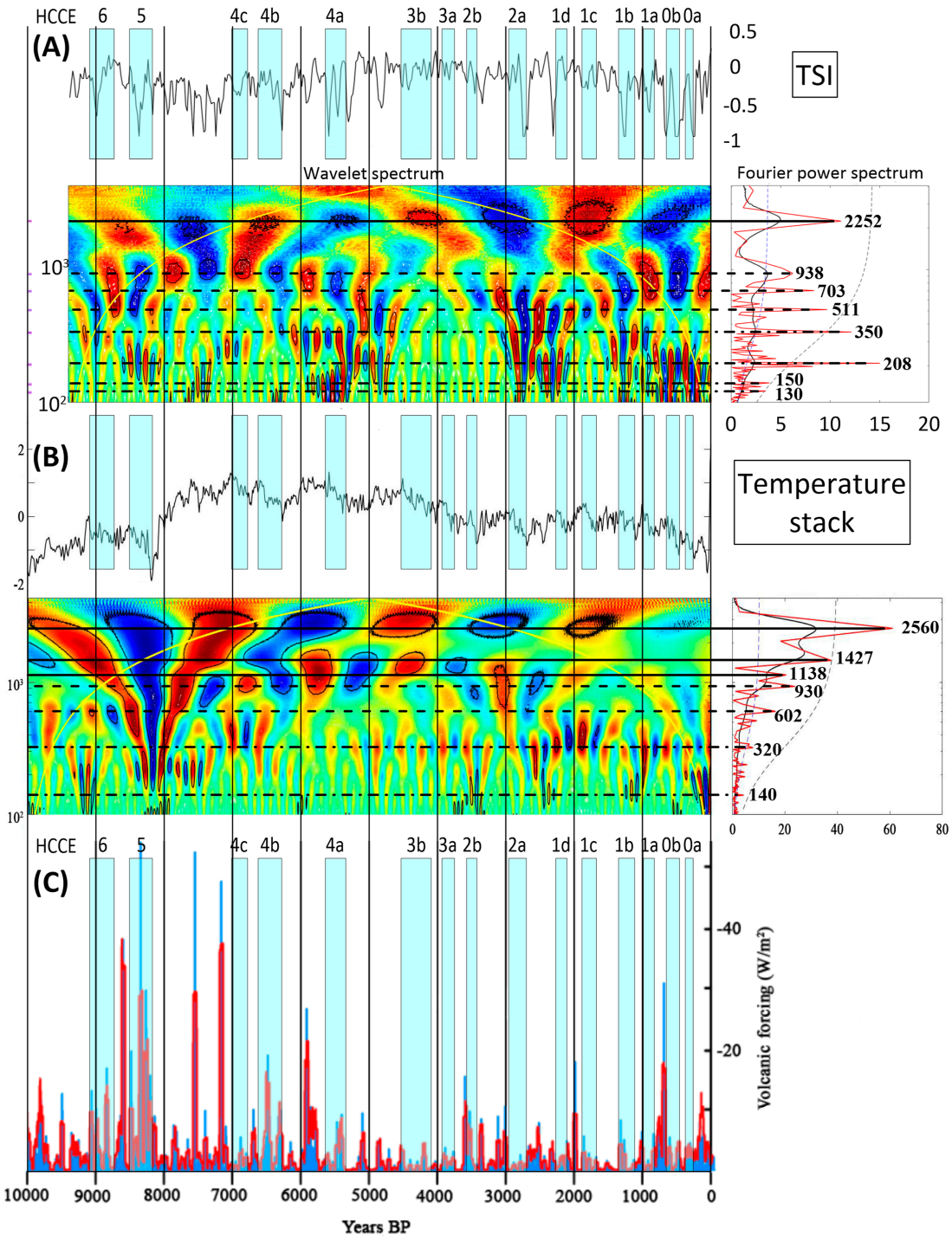

FIGURE 5
Time series, wavelet power spectra (left panels), and Fourier power spectrum (right panel) of **(A)** TSI (Steinhilber et al., 2012) and **(B)** synthesized climate stack (this study) over the last 10 ka using Morlet wavelet, normalized by 1/σ2. Wavelet analysis was performed using a MATLAB code for wavelet and Fourier spectrum calculations, developed based on published data (Torrence and Compo, 1998). The color gamut of the wavelet spectrum reflects the minima (blue color) and maxima (red color) of the wavelet decomposition coefficients, showing the temporal evolution of the amplitudes of the various periodicities. Black lines outline areas with a confidence level > 95% for a red-noise process with a lag^{-1} of α = 0.72. Yellow lines indicate the "cones of influence," where edge effects cannot be neglected. In the right panels, black solid lines indicate the global wavelet spectra, and red solid lines indicate the Fourier power spectra normalized by N/(σ2). Blue dashed lines are the mean red-noise spectra assuming a lag^{-1} of α = 0.72. Black dashed lines indicate the 95% confidence spectra. **(C)** Volcanic forcing record (Kobashi et al., 2017); the blue line indicates raw data (right scale), and the red line presents the 50-year window averaged data (left scale) of raw sulfate concentration in Greenland ice core GISP2 (Mayewski et al., 1997) modified by Kobashi et al. (2017). The centennial (120, 208, and 350 years), multi-centennial (500, 700, and 930 years), and millennial (1,130, 1,460, and 2,250–2,550 years) band periodicities are shown by chain, dotted, and solid lines, respectively **(A,B)**. Blue bars show the HCCEs, as shown in Figures 2–4.

Cosmic radiation variations, inferred from Earth's atmospheric radionuclide production, predominantly reflect solar modulation due to the correspondence between cosmic radiation maxima and grand solar minima (Steinhilber et al., 2012; Usoskin et al., 2016). Two distinct grand TSI minima types, shorter Maunder-type and longer Spörer-type, imply deterministic solar dynamo behavior likely governed by the combined gravitational energy influence of the Sun and closer planets (Simonenko, 2013; Scafetta et al., 2016; Usoskin et al., 2016). Small changes in the TSI and related ultraviolet radiation in the stratosphere may be transmitted downward into the troposphere, producing significant multi-decadal–centennial-scale changes in atmospheric circulation with significant impacts on global climate by "top-down" mechanisms; however, the "bottom-up" mechanisms of the Sun's influence have also been discussed (Shindell et al., 2001; Kodera and Kuroda, 2002; Haigh et al., 2005; Meehl et al., 2009; Gray et al., 2010; Connolly et al., 2021). In this study, we used two estimations of the TSI: longer and more robust estimations obtained by Steinhilber et al. (2012), based on the cosmic ray-produced radionuclides (^{10}Be and ^{14}C), and those by Egorova et al. (2018) that additionally incorporated the variability of sunspot umbra, sunspot penumbra, and faculae when available.

Stratospheric volcanic aerosols injected from explosive volcanism preclude the penetration of solar irradiance into Earth's surface and may have a strong effect on the climate and surface temperature despite their short residence time in the atmosphere (nearly 10 years or less) (Kobashi et al., 2017; Büntgen et al., 2020). Decadal-scale volcanic activity can induce multi-decadal–century cooling effects through the prolonged response times of the ocean surface water cooling and the expansion of sea ice following volcanic aerosol dispersion (Zhong et al., 2011; Sigl et al., 2015; 2022). In turn, explosive volcanic activity may be governed by the responses of the Earth's crust to the formation and retreat of vast masses of continental ice sheets, the Earth's dynamo evolution, or other external and internal factors.

Based on the measurements of the ^{231}Pa/^{230}Th ratio in a sediment core from the subtropical North Atlantic, a robust proxy of Atlantic meridional overturning circulation (AMOC), McManus et al. (2004) argued that AMOC was nearly, or completely, eliminated during the Heinrich Stadial 1, forced by large freshwater input into the North Atlantic due to the catastrophic iceberg discharge of the Laurentide ice sheet, and decreased sharply into the Younger Dryas cold event. They inferred that small changes in the hydrological cycle in the North Atlantic led to changes in AMOC and, in turn, to abrupt climate changes transmitted globally through atmospheric and oceanic feedbacks. Later, the measurements of two independent chemical water tracers (the isotope ratios of ^{231}Pa/^{230}Th and ^{143}Nd/^{144}Nd) in the North Atlantic ODP site 1063 obtained by Böhm et al. (2015) reveal consistent responses of the AMOC to the sequence of Heinrich stadials over the last glacial cycle through catastrophic iceberg discharges accompanied by freshwater pulses. This allows us to suggest that there is a persistent effect of the freshwater pulses into the North Atlantic on the significant or limited AMOC changes and, therefore, some influence on the global climate changes through the Pleistocene and Holocene, when large ice sheets covered the NH continents.

It is believed that ENSO, a coupled ocean–atmosphere instability in the tropical Pacific with vast heat storage in upper waters (200 m) and strong positive feedback between the atmosphere and upper ocean, possesses significant potential for inducing global climate shifts in the past, present, and future (Bjerknes, 1969; Wang et al., 2001; Cane, 2005). Several studies suggest that the dominant external forcing of ENSO variability, related to the frequency and magnitude of El Niño events, is a seasonal change in solar insolation coming into the low latitudes, which is governed by Earth's orbit geometry (Münnich et al., 1991; Chang et al., 1994; Tziperman et al., 1997; Cane, 2005).

Over the last precession cycle, minimal differences in incoming solar insolation between winter and summer seasons in low-latitude regions occurred at approximately 12–8 kyr BP, gradually intensifying since 6–5 kyr BP, implying a coeval strengthening of ENSO variability (Clement et al., 2000; Cane, 2005). ENSO variability records derived from Laguna Pallcacocha in southern Ecuador (Moy et al., 2002) and El Junco Lake in the Galapagos Islands (Conroy et al., 2008) demonstrate low ENSO variability during the early Holocene, with a slight intensification approximately 7 kyr BP. ENSO variability was also subdued at the start of the middle Holocene, escalating from nearly 4 kyr BP, marked by several strong spikes over 2–0.5 kyr BP. This is consistent with ENSO reconstruction based on foraminifera chemistry from a marine sediment core, revealing relatively low-amplitude ENSO variability between 5.5 and 10 ka BP (White et al., 2018). This trend aligns with theoretical and modeled reconstructions of ENSO variability over the Holocene, showing minimal ENSO variability during the early Holocene and gradual intensification since 5–6 kyr BP (Koutavas and Joanides, 2012; Cobb et al., 2013; Sadekov et al., 2013; Carré et al., 2014). The intensification of ENSO variability likely contributed to warmer conditions in the eastern equatorial Pacific and colder conditions in the western region, accompanied by EASM weakening and decreased precipitation in eastern Asia.

ODP site 1002, investigated by Haug et al. (2001), is situated within the Cariaco Basin off the Venezuelan coast within the northern boundary of the ITCZ. This location is significant because the modern boreal summer/winter migration of the ITCZ recorded in site 1002 exhibits lesser seasonal shifting, contrary to those in the Indian Ocean. Therefore, fluctuations in the Ti content of this core allow for the sensitive monitoring of the meridional migration of the northern boundary of the ITCZ in the past. On the centennial–millennial time scale, the boreal–summer ITCZ appears to have migrated southward in line with NH cooling, which, in turn, is governed by Earth orbit geometry (Koutavas and Joanides, 2012; Schneider et al., 2014). An ITCZ meridional shifting, or its contraction/expansion in the latitudinal range over climate changes, regulates tropical heat distribution between hemispheres through surface water currents and atmospheric circulation (Conroy et al., 2008; Schneider et al., 2014; Yan et al., 2015).

Two EASM records obtained from the Sanbao (Dong et al., 2010) and Dongge caves (Wang et al., 2005), located in the eastern part of China, reflect changes in hydrological processes of the tropical Pacific and Indian Ocean by moisture transport into Eastern Asia, extending up to Japan and southeastern Russia (Wang et al., 2001; 2005; Cheng et al., 2012). These changes were associated with a seasonal reversal in surface winds and shifts in precipitation associated with the seasonal migration of the ITCZ (Dong et al., 2010; Cheng et al., 2012; Wang et al., 2017). It appears that the

temporal variability of the EASM recorded from China was better defined by changes in the intensity and extension of the Western Pacific Warm Pool, also affected by ENSO variability.

The Siberian High (SH) atmospheric center during the winter season covers a large area of the Eurasian continent at mid–high latitudes and combines vast masses of cold air at the NH. The variability of the SH and the related upper atmosphere Northern Hemispheric Westerlies (NWs) during the Holocene were reconstructed based on terrigenous K^+ ion content in Greenland ice core GISP2 (Mayewski et al., 2004). Higher SH/NWs create favorable conditions for the emergence of widespread NH cold events, attributed to the impact of weak external or internal triggers on the climate system.

4.3 Sequence of the outlined HCCEs through the Holocene and their origins

To understand the forcing mechanisms behind the outlined HCCEs in the NH, we compared the constructed climate stack and detected HCCEs with potential climate forcings—TSI (Steinhilber et al., 2012; Egorova et al., 2018), AMOC variability recorded in the $^{231}Pa/230^{Th}$ ratio from deep-sea sediments (Hoffmann et al., 2018), meridional shifting of the ITCZ (Haug et al., 2001), and ENSO variabilities recorded in the Laguna Pallcacocha (Moy et al., 2002) and El Junco Lake (Conroy et al., 2008) (Figures 4B, C, E, F, K). Kobashi et al. (2017) presented a record of explosive volcanic activity variability in the NH based on the modifications of the sulfate concentration in the Greenland ice core GISP2 (Mayewski et al., 1997). Based on sulfur measurements in the Greenland and Antarctica ice cores, Sigl et al. (2022) revealed the global estimation of the sulfur injection into the stratosphere by volcanic eruptions during the Holocene. The authors showed that from the total volcanic sulfur injected into the stratosphere, 70% originate from tropical eruptions and 25% from NH extratropical eruptions due to a bipolar difference in volcanic eruption distribution. Therefore, the record of volcanic activity obtained by Kobashi et al. (2017) is closely aligned with the globally inferred record obtained by Sigl et al. (2022), which we accept as evidence of volcanic activity forcing.

As evidence of AMOC variability as a climate forcing over the Holocene, we accept the $^{231}Pa/230^{Th}$ ratio measured in the sediment core at an intermediate depth from the North Atlantic (Hoffmann et al., 2018) as a more sensitive record of the AMOC formation changes, in contrast to that from the deep-sea sediment core obtained by McManus et al. (2004). Additionally, we incorporated the SH/NW records from the Greenland ice core (Mayewski et al., 2004) and the EASM stack, both representing the evolution of the NH main atmospheric circulation centers, along with the classical Greenland temperature record (Rasmussen et al., 2014) (Figures 4D, G, J).

HCCEs 6 and 5 were accompanied by the coeval superposition of the TSI minima and strong multi-decadal increases in explosive volcanism (Figures 4H, I), both contributing to a decrease in solar radiation on Earth's surface and, therefore, NH climate cooling. However, HCCE 5 was also terminated by a certain increase in the $^{231}Pa/^{230}Th$ ratio in the sediment of the Atlantic core (Figure 4B), indicating a limited decrease in the AMOC (Hoffmann et al., 2018; Lippold et al., 2019). The freshwater pulse into the North Atlantic at 8.2 ka BP is also consistent with evidence of coeval accelerated collapsing of the Laurentide ice sheet in North America (Clark et al., 2001; Matero et al., 2017). HCCE 5 was mostly likely driven by freshening of the North Atlantic surface and limited AMOC slowdown, superimposed on the coeval TSI minima, and increases in explosive volcanism, leading to the globally extended 8.2-ka cold event (Clark et al., 2001; Alley and Agustsdottir, 2005; Carlson et al., 2008; Cheng et al., 2009; Rasmussen et al., 2014; Matero et al., 2017; Doring and Leuenberger, 2022; Duan et al., 2023).

The period between HCCEs 5 and 4a (8.16–5.62 kyr BP), often referred to as the HTM (Geirsdóttir et al., 2013; Marcott et al., 2013; Brooks et al., 2015; Kobashi et al., 2017; Hou et al., 2019; Kaufman and Broadman, 2023), exhibits pronounced temperature contrasts between the Northern and Southern Hemispheres in poleward regions of 30°N and 30°S, as reconstructed by Marcott et al. (2013), indicating a period of significant warmth of the NH (Figure 4A). The HTM was also marked by weak SH/NW and strong EASM formations related to warmer climatic conditions of the NH (Figures 4G, J). However, according to the synthesized temperature stack, the HTM was punctuated by HCCEs 4c and 4b. HCCEs 4c and 4b were accompanied by a coeval significant southward shift of the ITCZ, a certain decrease in the NH-SH temperature contract, and weakening of the EASM, likely related to cooling in the tropical area (Figures 4C, G, J). Moy et al. (2002) and Conroy et al. (2008) revealed some initial intensification of El Niño variability at approximately 7 kyr BP, coinciding with these tropical processes and aligning with some increase in seasonal differences in solar insolation at the low-latitude regions (Figures 4A, E). Significant multi-decadal peaks of volcanic activity during HCCE 4b, likely initiated these cooling events (Figure 4H). Notably, during HCCEs 4c and 4b, TSI values decreased insignificantly (Figure 4I). Therefore, climate cooling over HCCEs 4c and 4b, was most likely initiated by significant processes in the tropical zone, such as intensification of ENSO variability, southward ITCZ shifting, and EASM weakening that started to decrease the temperature contrast between the Northern and Southern Hemispheres during the HTM (Figures 4A, C, E, J).

HCCE 4a (5.64–5.34 kyr BP), accompanied by significant TSI minimum and some heightened explosive volcanic activity, had terminated the HTM and likely corresponded to highlighting the combined influence of solar factors and volcanism (Figures 4H, I). HCCE 4a occurred during the weakening of the EASM activity and the highest SH/NW values, which facilitated climate cooling initiated by external and internal forcings (Figures 4G, J).

The MHO, observed by Kobashi et al. (2017), occurred between HCCEs 4a and 3a during 5.34–3.94 kyr BP. Incorporated into the MHO, HCCE 3b was characterized by two cooling events, separated by small short-term stable conditions (Figures 2L, M). Nevertheless, this cooling was accompanied by a remarkable southward shift in the ITCZ, likely related to the initiation of significant processes in the tropical zone, as supported by the coeval decrease in the EASM activity (Figure 4C).

HCCEs 3a and 2b were accompanied by a certain decrease in TSIs; however, they were marked by a remarkable southward shift in the ITCZ, EASM weakening, and a decrease in the

NH-SH temperature contrast (Figures 4A, C, I, J). Notably, these important changes in Earth's climate system over the HCCEs 3b–3a–2b (4.53–3.42 ka BP) were also accompanied by a significant strengthening of the ENSO variability, according to Conroy et al. (2008) and White et al. (2018), leading to the significant reorganization of the Holocene climate, consistently with a significant decrease in the NH-SH temperature contrast and increase in seasonal insolation differences at the tropical areas (Figures 4A, E, F). The strengthening of the ENSO variability approximately 4 kyr BP led to warmer surface waters in the eastern equatorial Pacific, cooling in the western Pacific, and weakening of EASM formation in the western equatorial Pacific, resulting in decreased evaporation and moisture delivery to East Asia. Sun et al. (2019) investigated 130 well-dated geological records from sites located in climatically and topographically different regions of China and found dramatic climate changes related to extreme hydrological events in different regions of China, leading to the collapse of major, well-documented Chinese Neolithic cultures—approximately 4 kyr BP. The authors suggest that the destruction of Neolithic cultures in China and unfavorable living conditions were driven by decreasing warmth and wetness in the arid and semi-arid regions of China. A remarkable increase in ENSO variability and southward shifts in the ITCZ over HCCEs 3b, 3a, and 2b, accompanied by a temperature rearrangement between the Northern and Southern Hemispheres, were likely the main causes of the destruction of Neolithic cultures in China and the onset of the Neoglacial period of the Holocene (Figures 4A, C). The record of quartz content obtained by Moros et al. (2006) shows coeval cooling of the northwestern Atlantic environment (Figure 2E) during HCCEs 3b, 3a, and 2b, supporting the NH cooling since the Neoglacial period. HCCE 2b was forced by the significant intensification of explosive volcanism, leading to a decrease in the input of solar insolation to the Earth's surface (Figure 4H).

HCCE 2a (2.96–2.70 ka BP) occurred during the maximum of SH/MW in NH atmosphere circulation, resulting in Earth climate cooling, consistent with the decrease in the Greenland temperature and weakening of the EASM (Figures 4D, G, J). This remarkable Homeric TSI minimum (HGSM) was likely the main driver of HCCE 2a (Figure 4I).

Subsequent HCCEs 1d–0a were accompanied or preceded by minima in coming solar insolation with variable intensities, along with strengthening ENSO variability (Figures 4E, I). These external and internal forcings were likely the main drivers of Earth's climate cooling over the last 2 ka. Recent HCCEs 0b and 0a, preceded by intensification of volcanic activity, occurred during strong Sporer and Maunder solar grand minima, respectively, and remarkable maxima of the SH/NW in the NH atmosphere circulation (Figures 4G–I). As a result, the ages of HCCEs 0b and 0a are close to the onset of the LIA formation.

A comparison of the established HCCEs with potential drivers of the Holocene climate changes suggests that the temperature variability within the lower troposphere of the NH may be mostly explained in terms of solar variability, volcanic activity, and ITCZ/ENSO variability, consistent with the conclusion obtained by Soon et al. (2000), while initial HCCEs 6 and 5 were likely forced by AMOC influence.

4.4 Wavelet diagrams and spectral power density of the constructed climate stack and TSI and climate-dominated forcing

The Fourier spectral power of the TSI (Steinhilber et al., 2012) reveals centennial band periodicities at 130 years, 150 years, 208 years (very close to the well-known 205-year de Vries cycle), and 350 years, multi-centennial periodicities at 511 years, 703 years, and 938 years (Eddy cycle), and millennial scale of 2,252 years (Figure 5A, right side), aligning with TSI periodicities presented by Abreu et al. (2012).

Notably, the longest TSI cycle corresponds closely to the astronomical origin of the Hallstatt cycle found in the Holocene by Scafetta et al. (2016). The Hallstatt cycle frequency is influenced by the evolution of the Sun's planetary mass center alongside larger planets like Jupiter, Saturn, Uranus, and Neptune, whose rotations oscillate with variable periodicities of 2,100–2,500 years (Scafetta et al., 2016).

The wavelet diagram of the TSI proposed by Steinhilber et al. (2012) showed that the centers of the strongest amplitudes of higher-frequency cycles (130, 150, 208, and 350 years) predominately vary throughout the Holocene with an average timing of approximately 8.2, 5.5, 2.6, and 0.7 kyr BP (Figure 5A, chain lines). Such periodicities with the strongest amplitudes in high-frequency TSI cycles are nearly close to the maxima of the SH/NW in atmospheric circulation (Figure 4G), indicating its causal linkages with atmospheric circulation at the NH.

The spectral power of the constructed temperature stack showed changes with centennial periodicities of 140 and 320 years, multi-centennial bands of 602 and 930 years, and millennial cycles of 1,138, 1,427, and 2,560 years, which resemble periodicities of the TSI record (Figure 5B, chain lines). However, according to the wavelet diagram of the temperature stack, the temporal evolution of the amplitudes of the centennial (100–350 years), multi-centennial band (500–930 years), and millennial-band periodicities significantly differed from those of the TSI cycles (Figures 5A, B, chain, dotted, and solid lines, respectively). The temporal evolution of the amplitudes of the centennial (100–350 years) cycles in the temperature stack reveals itself to be much weaker between the 7 and 3 ka BP than those of the TSI. This indicates that factors other than solar activity influence the Holocene climate changes. Millennial periodicities of the temperature stack, such as 1,138 years and 1,427 years, appear in the wavelet diagram of the temperature stack, contrary to the Fourier and wavelet spectra of the TSI record (Figures 5A, B). These millennial periodicities of temperature stacks may be formed as the heterodyne response of Earth's climate system to centennial-scale TSI forcing (Clemens, 2005), for example, 1/350–1/511= 1/1111. The Hallstatt cycle (2,250–2,550 years) seems to be observed in both the temperature stack and TSI record.

Figure 5C demonstrates the significant influence of volcanic eruptions on the climate and formation of HCCEs (Figures 5B, C) when intensification of volcanisms preceded or occurred during the HCCEs. For example, the series of abrupt and large intensifications of volcanisms between 9.1 and 8.1 kyr BP likely facilitate the formation of HCCEs 6 and 5, along with other forcings—TSI minima and AMOC-limited slowdown. A strong increase in volcanisms over 5.95–5.40 kyr BP may also force the termination of the HTM around HCCE 4a, together with

the TSI driver (Figures 5A, C; 4H). Remarkably, the pronounced intensification of explosive volcanism over nearly 800–600 years BP and after 400 years BP likely served as a primary driving force behind the LIA (HCCEs 0a and 0b) (Figure 5C). A comparison of the wavelet diagrams of the TSI and temperature stack with volcanic activity (Figures 5A–C) indicates the significant influence of volcanic eruptions on the Holocene climate in the NH, consistent with the study by Kobashi et al. (2017) and Büntgen et al. (2020).

The pattern and chronology of the synthesized temperature stack and, therefore, of the HCCEs are limited by the uncertainties and temporal resolution of the time series used, which is estimated as several decades. An additional uncertainty in the age boundaries of the identified HCCEs is introduced by the incomplete synchronization of time series with each other. Obtaining new high-resolution and well-dated records of Holocene climate changes in the NH with the identification of new robust time markers of the Holocene will help clarify the chronology of the centennial climate cooling presented in this work and provide insights into the external and internal drivers behind them.

5 Conclusion

In this study, we used eight highly resolved and best-dated published temperature and climate records from different climatic zones, utilizing various proxies, to construct a Holocene marine–coastal temperature stack in the NH. To this end, we used the original age models of these records, with minor modifications for two them. Based on the constructed temperature stack, we established the chronology of 15 prominent HCCEs, periods with decreased temperature: 0a, 0b, 1a, 1b, 1c, 1d, 2a, 2b, 3a, 3b, 4a, 4b, 4c, 5, and 6, following the numbering from Bond cycles, each lasting 1–4 centuries over the last 10 kyr.

To test the chronological validity of the constructed HCCEs, we compared them with the best-dated and highly resolved temperature records of the NH and variability of the main centers of atmospheric circulation (NAO and SH/NW) and EASM over the last 3 kyr. Based on the nearly close alignment of the outlined HCCEs 2a, 1d, 1c, 1b, 1a, 0b, and 0a with the mentioned temperature records in the NH, as well as their correspondence to the main variability of atmospheric circulation over the last 3 kyr, we suggest that other HCCEs also correspond to centennial climate cooling in the NH over the last 10 kyr.

The synthesized Holocene centennial climate change stack and outlined HCCEs broadly correspond to major established Holocene climate events in the NH: the 8.2-kyr BP cooling, HTM, MHO, collapse of Chinese Neolithic cultures, 2.8-kyr BP cooling linked to the HGSM, and LIA. However, established HCCEs indicate a higher resolution of centennial-scale climate cooling during the Holocene and allow for a better understanding of the underlying force.

To understand the external and internal natural forcings of the Holocene temperature decreases in the NH, we conducted a comparative analysis of the sequence of outlined HCCEs with potential climate drivers responsible for them. These included the TSI record, explosive volcanic activity, AMOC formation changes, ITCZ fluctuations, ENSO variability, and related NH atmospheric circulation changes recorded in the EASM and SH/NW curves. For example, the recognized 8.2-kyr BP cooling event (HCCE 5) was likely driven by the superposition of the AMOC-limited slowdown, TSI minimum, and volcanic activity. However, HCCEs 3b, 3a, and 2b (over 4.53–3.42 BP), accompanied by small changes in the TSI, were likely mainly forced by an increase in ENSO variability, leading to remarkable changes in the tropical processes and a southward shift in the ITCZ, coeval with the collapse of the Chinese Neolithic cultures and the onset of the Holocene Neoglacial. The RWP and MWP experienced abrupt and robust warming over several decades, followed by gradual cooling spanning several centuries outlined by HCCEs 1c and 1a, respectively, and concluded by mild warms. Subsequent HCCEs 0b and 0a were likely forced by the TSI minimum combined with the increased role of ENSO and volcanism over the LGM. Therefore, the outlined HCCEs reflect the complicated origin of Holocene climate changes governed by the variability of Earth's orbital geometry, sunspot dynamics, and the evolving interplay between the Sun and Earth within the gravitational field of the solar system.

Data availability statement

The original contributions presented in the study are included in the article/Supplementary Material, further inquiries can be directed to the corresponding author.

Author contributions

SG: Conceptualization, Methodology, Supervision, Writing–original draft. XS: Supervision, Validation, Writing–review and editing. YL: Data curation, Resources, Writing–review and editing. AB: Data curation, Visualization, Writing–review and editing. YV: Formal Analysis, Methodology, Writing–review and editing. AA: Funding acquisition, Supervision, Writing–review and editing. EY: Investigation, Methodology, Writing–review and editing. JZ: Resources, Supervision, Writing–review and editing. ZY: Formal Analysis, Software, Writing–review and editing. IK: Validation, Visualization, Writing–review and editing.

Funding

The author(s) declare that financial support was received for the research, authorship, and/or publication of this article. The cruise during which the studied core was obtained and the primary processing onboard the ship was financially supported by the Laoshan Laboratory (LSKJ202204203), the Taishan Scholar Program of Shandong (tspd20181216), and the Russian state budget (number 121021700342–9 of the POI FEB RAS). Part of the work was conducted on the state assignment of the IGM SB RAS. Laboratory and analytical processing of samples and preparation and writing of the manuscript were fully funded by the Russian Science Foundation (number 22–17–00118).

Conflict of interest

The authors declare that the research was conducted in the absence of any commercial or financial relationships that could be construed as a potential conflict of interest.

Publisher's note

All claims expressed in this article are solely those of the authors and do not necessarily represent those of their affiliated organizations, or those of the publisher, the editors, and the reviewers. Any product that may be evaluated in this article, or claim that may be made by its manufacturer, is not guaranteed or endorsed by the publisher.

Supplementary material

The Supplementary Material for this article can be found online at: https://www.frontiersin.org/articles/10.3389/feart.2024.1415180/full#supplementary-material

References

Abreu, J. A., Beer, J., Ferriz-Mas, A., McCracken, K. G., and Steinhilber, F. (2012). Is there a planetary influence on solar activity? *Astron. Astrophys.* 548, A88. doi:10.1051/0004-6361/201219997

Alley, R. B., and Agustsdottir, A. M. (2005). The 8k event: cause and consequences of a major Holocene abrupt climate change. *Quat. Sci. Rev.* 24, 1123–1149. doi:10.1016/j.quascirev.2004.12.004

Alley, R. B., Meese, D. A., Shuman, C. A., Gow, A. J., Taylor, K. C., Grootes, P. M., et al. (1993). Abrupt increase in Greenland snow accumulation at the end of the Younger Dryas event. *Nature* 362, 527–529. doi:10.1038/362527a0

Bailey, H. L., Kaufman, D. S., Sloane, H. J., Hubbard, A. L., Henderson, A. C. G., Leng, M. J., et al. (2018). Holocene atmospheric circulation in the central North Pacific: a new terrestrial diatom and δ18O dataset from the Aleutian Islands. *Quat. Sci. Rev.* 194, 27–38. doi:10.1016/j.quascirev.2018.06.027

Berger, A. L. (1978). Long-term variations of caloric insolation resulting from the earth's orbital elements. *Quat. Res.* 9, 139–167. doi:10.1016/0033-5894(78)90064-9

Berger, A. L., Loutre, M.-F., and Tricot, C. (1993). Insolation and Earth's orbital periods. *J. Geophys. Res.* 98, 10341–10362. doi:10.1029/93JD00222

Bjerknes, J. (1969). Atmospheric teleconnections from the equatorial Pacific. *Mon. Weather Rev.* 97, 163–172. doi:10.1175/1520-0493(1969)097<0163:atftep>2.3.co;2

Böhm, E., Lippold, J., Gutjahr, M., Frank, M., Blaser, P., Antz, B., et al. (2015). Strong and deep Atlantic meridional overturning circulation during the last glacial cycle. *Nature* 517, 73–76. doi:10.1038/nature14059

Bond, G. C., Kromer, B., Beer, J., Muscheler, R., Evans, M. N., Showers, W., et al. (2001). Persistent solar influence on North Atlantic climate during the holocene. *Science* 294, 2130–2136. doi:10.1126/science.1065680

Briffa, K. R., Osborn, T. J., Schweingruber, F. H., Harris, I. C., Jones, P. D., Shiyatov, S. G., et al. (2001). Low-frequency temperature variations from a northern tree ring density network. *J. Geophys. Res. Atmos.* 106, 2929–2941. doi:10.1029/2000JD900617

Brooks, S. J., Diekmann, B., Jones, V. J., and Hammarlund, D. (2015). Holocene environmental change in Kamchatka: a synopsis. *Glob. Planet. Change* 134, 166–174. doi:10.1016/j.gloplacha.2015.09.004

Buckley, M. W., and Marshall, J. (2016). Observations, inferences, and mechanisms of the atlantic meridional overturning circulation: a review. *Rev. Geophys.* 54, 5–63. doi:10.1002/2015RG000493

Büntgen, U., Arseneault, D., Boucher, E., Churakova (Sidorova), O. V., Gennaretti, F., Crivellaro, A., et al. (2020). Prominent role of volcanism in Common Era climate variability and human history. *Dendrochronologia* 64, 125757. doi:10.1016/j.dendro.2020.125757

Büntgen, U., Frank, D. C., Nievergelt, D., and Esper, J. (2006). Summer temperature variations in the European Alps, a.d. 755–2004. *J. Clim.* 19, 5606–5623. doi:10.1175/JCLI3917.1

Büntgen, U., Tegel, W., Nicolussi, K., McCormick, M., Frank, D., Trouet, V., et al. (2011). 2500 Years of European climate variability and human susceptibility. *Science* 331, 578–582. doi:10.1126/science.1197175

Cane, M. A. (2005). The evolution of El Niño, past and future. *Earth Planet. Sci. Lett.* 230, 227–240. doi:10.1016/j.epsl.2004.12.003

Carlson, A. E., LeGrande, A. N., Oppo, D. W., Came, R. E., Schmidt, G. A., Anslow, F. S., et al. (2008). Rapid early Holocene deglaciation of the Laurentide ice sheet. *Nat. Geos* 1, 620–624. doi:10.1038/ngeo285

Carré, M., Sachs, J. P., Purca, S., Schauer, A. J., Braconnot, P., Falcón, R. A., et al. (2014). Holocene history of ENSO variance and asymmetry in the eastern tropical Pacific. *Science* 345, 1045–1048. doi:10.1126/science.1252220

Chang, P., Wang, B., Li, T., and Ji, L. (1994). Interactions between the seasonal cycle and the Southern Oscillation - frequency entrainment and chaos in a coupled ocean-atmosphere model. *Geophys. Res. Lett.* 21, 2817–2820. doi:10.1029/94GL02759

Cheng, H., Edwards, R. L., Broecker, W. S., Denton, G. H., Kong, X., Wang, Y., et al. (2009). Ice age terminations. *Science* 326, 248–252. doi:10.1029/94GL02759

Cheng, H., Sinha, A., Wang, X., Cruz, F. W., and Edwards, R. L. (2012). The global paleomonsoon as seen through speleothem records from Asia and the americas. *Clim. Dyn.* 39, 1045–1062. doi:10.1007/s00382-012-1363-7

Clark, P. U., Marshall, S. J., Clarke, G. K. C., Hostetler, S. W., Licciardi, J. M., and Teller, J. T. (2001). Freshwater forcing of abrupt climate change during the last glaciation. *Science* 293, 283–287. doi:10.1126/science.1062517

Clemens, S. C. (2005). Millennial-band climate spectrum resolved and linked to centennial-scale solar cycles. *Quat. Sci. Rev.* 24, 521–531. doi:10.1016/j.quascirev.2004.10.015

Clement, A. C., Seager, R., and Cane, M. A. (2000). Suppression of El Niño during the mid-holocene by changes in the earth's orbit. *Paleoceanography* 15, 731–737. doi:10.1029/1999PA000466

Cobb, K. M., Westphal, N., Sayani, H. R., Watson, J. T., Di Lorenzo, E., Cheng, H., et al. (2013). Highly variable El niño–southern oscillation throughout the holocene. *Science* 339, 67–70. doi:10.1126/science.1228246

Connolly, R., Soon, W., Connolly, M., Baliunas, S., Berglund, J., Butler, C. J., et al. (2021). How much has the Sun influenced Northern Hemisphere temperature trends? An ongoing debate. *Res. Astronomy Astrophysics* 21, 131. doi:10.1088/1674-4527/21/6/131

Conroy, J. L., Overpeck, J. T., Cole, J. E., Shanahan, T. M., and Steinitz-Kannan, M. (2008). Holocene changes in eastern tropical Pacific climate inferred from a Galápagos lake sediment record. *Quat. Sci. Rev.* 27, 1166–1180. doi:10.1016/j.quascirev.2008.02.015

Corrick, E. C., Drysdale, R. N., Hellstrom, J. C., Capron, E., Rasmussen, S. O., Zhang, X., et al. (2020). Synchronous timing of abrupt climate changes during the last glacial period. *Science* 369, 963–969. doi:10.1126/science.aay5538

Dansgaard, W., Johnsen, S. J., Clausen, H. B., Dahl-Jensen, D., Gundestrup, N. S., Hammer, C. U., et al. (1993). Evidence for general instability of past climate from a 250-kyr ice-core record. *Nature* 364, 218–220. doi:10.1038/364218a0

deMenocal, P., Ortiz, J., Guilderson, T., and Sarnthein, M. (2000). Coherent high- and low-latitude climate variability during the holocene Warm Period. *Science* 288, 2198–2202. doi:10.1126/science.288.5474.2198

Denton, G. H., and Karlén, W. (1973). Holocene climatic variations—their pattern and possible cause. *Quat. Res.* 3, 155–205. doi:10.1016/0033-5894(73)90040-9

Dong, J., Wang, Y., Cheng, H., Hardt, B., Edwards, R. L., Kong, X., et al. (2010). A high-resolution stalagmite record of the Holocene East Asian monsoon from Mt Shennongjia, central China. *Holocene* 20, 257–264. doi:10.1177/0959683609350393

Döring, M., and Leuenberger, M. C. (2022). Comparison of Holocene temperature reconstructions based on GISP2 multiple-gas-isotope measurements. *Quat. Sci. Rev.* 280, 107274. doi:10.1016/j.quascirev.2021.107274

Duan, F., Zhang, Z., Liu, D., Chen, J., Shao, Q., and Wang, Y. (2023). Stalagmite-based long-term and multi-centennial hydroclimatic variations in southwestern China during the Holocene and relations to global climate change. *Clim. change Quat. Sci. Rev.* 319, 108327. doi:10.1016/j.quascirev.2023.108327

Egorova, T., Schmutz, W., Rozanov, E., Shapiro, A. I., Usoskin, I., Beer, I. J., et al. (2018). Revised historical solar irradiance forcing. *Astronomy and Astrophysics* 615, A85. doi:10.1051/0004-6361/201731199

Esper, J., Cook, E. R., and Schweingruber, F. H. (2002). Low-frequency signals in long tree-ring chronologies for reconstructing past temperature variability. *Science* 295, 2250–2253. doi:10.1126/science.1066208

Geirsdóttir, Á., Miller, G. H., Larsen, D. J., and Ólafsdóttir, S. (2013). Abrupt holocene climate transitions in the northern north atlantic region recorded by synchronized lacustrine records in Iceland. *Quat. Sci. Rev.* 70, 48–62. doi:10.1016/j.quascirev.2013.03.010

Gorbarenko, S. A., Goldberg, E. L., Kashgarian, M., Velivetskaya, T. A., Zakharkov, S. P., Pechnikov, V. S., et al. (2007). Millennium scale environment changes of the Okhotsk Sea during last 80 kyr and their phase relationship with global climate changes. *J. Oceanogr.* 63, 609–623. doi:10.1007/s10872-007-0054-1

Gorbarenko, S. A., Shi, X., Malakhova, G. Y., Bosin, A. A., Zou, J., Liu, Y., et al. (2017). Centennial to millennial climate variability in the far northwestern pacific (off kamchatka) and its linkage to the East Asian monsoon and North Atlantic from the last glacial maximum to the early holocene. *Clim. Past.* 13, 1063–1080. doi:10.5194/cp-13-1063-2017

Goslar, T. (2003). 14C as an indicator of solar variability. *PAGES news* 11, 12–14. doi:10.22498/pages.11.2-3.12

Gray, L. J., Beer, J., Geller, M., Haigh, J. D., Lockwood, M., Matthes, K., et al. (2010). Solar influences on climate. *Rev. Geophys.* 48, RG4001. doi:10.1029/2009RG000282

Haigh, J. D., Lockwood, M., and Giampapa, M. S. (2005). in *The Sun, solar analogs and the climate*. Editors I. Rüedi, W. Schmutz, and M. Güdel (Berlin/Heidelberg: Springer-Verlag). doi:10.1007/3-540-27510-X

Harding, P., Martin-Puertas, C., Sjolte, J., Walsh, A. A., Tjallingii, R., Langdon, C., et al. (2023). Wind regime changes in the euro-atlantic region driven by late-holocene grand solar minima. *Clim. Dyn.* 60, 1947–1961. doi:10.1007/s00382-022-06388-w

Haug, G. H., Hughen, K. A., Sigman, D. M., Peterson, L. C., and Röhl, U. (2001). Southward migration of the intertropical convergence zone through the Holocene. *Science* 293, 1304–1308. doi:10.1126/science.1059725

Herzschuh, U., Böhmer, T., Chevalier, M., Hébert, R., Dallmeyer, A., Li, C., et al. (2023). Regional pollen-based Holocene temperature and precipitation patterns depart from the Northern Hemisphere mean trends. *Clim. Past.* 19, 1481–1506. doi:10.5194/cp-19-1481-2023

Hoffmann, S. S., McManus, J. F., and Swank, E. (2018). Evidence for stable Holocenebasin-scale overturning circulationdespite variable currents along thedeep western boundary of the NorthAtlantic Ocean. *Geophys. Res. Lett.* 45 (13), 427–436. doi:10.1029/2018GL080187

Hou, J., Li, C.-G., and Lee, S. (2019). The temperature record of the Holocene: progress and controversies. *Sci. Bull.* 64, 565–566. doi:10.1016/j.scib.2019.02.012

Kaniewski, D., Paulissen, E., Van Campo, E., Weiss, H., Otto, T., Bretschneider, J., et al. (2010). Late second–early first millennium BC abrupt climate changes in coastal Syria and their possible significance for the history of the Eastern Mediterranean. *Quat. Res.* 74, 207–215. doi:10.1016/j.yqres.2010.07.010

Kaufman, D. S., and Broadman, E. (2023). Revisiting the Holocene global temperature conundrum. *Nature* 614, 425–435. doi:10.1038/s41586-022-05536-w

Kobashi, T., Menviel, L., Jeltsch-Thömmes, A., Vinther, B. M., Box, J. E., Muscheler, R., et al. (2017). Volcanic influence on centennial to millennial Holocene Greenland temperature change. *Sci. Rep.* 7, 1441. doi:10.1038/s41598-017-01451-7

Kodera, K., and Kuroda, Y. (2002). Dynamical response to the solar cycle. *J. Geophys. Res. Atmos.* 107. doi:10.1029/2002JD002224

Koutavas, A., and Joanides, S. (2012). El niño-southern oscillation extrema in the holocene and last glacial maximum. *Paleoceanography* 27. doi:10.1029/2012PA002378

Li, Q., Zhang, Q., Li, G., Liu, Q., Chen, M.-T., Xu, J., et al. (2019). A new perspective for the sediment provenance evolution of the middle Okinawa Trough since the last deglaciation based on integrated methods. *Earth Planet. Sci. Lett.* 528, 115839. doi:10.1016/j.epsl.2019.115839

Lippold, J., Pöppelmeier, F., Süfke, F., Gutjahr, M., Goepfert, T. J., Blaser, P., et al. (2019). Constraining the variability of the Atlantic meridional overturning circulation during the holocene. *Geophys. Res. Lett.* 46 (11), 11338–11346. doi:10.1029/2019GL084988

Liu, Z., Zhu, J., Rosenthal, Y., Zhang, X., Otto-Bliesner, B. L., Timmermann, A., et al. (2014). The Holocene temperature conundrum. *Proc. Natl. Acad. Sci.* 111, E3501–E3505. doi:10.1073/pnas.1407229111

Ljungqvist, F. C. (2010). A new reconstruction of temperature variability in the extra-tropical northern hemisphere during the last two millennia. *Geogr. Ann. Ser. A, Phys. Geogr.* 92, 339–351. doi:10.1111/j.1468-0459.2010.00399.x

Ma, H., Zeng, S., Chen, L., He, J., Yin, M., Zeng, X., et al. (2008). History of heavy metals recorded in the sediment of the Chukchi Sea, Arctic. *J. Oceanogr. Taiwan Strait* 27, 15–50.

Mann, M. E., Zhang, Z., Hughes, M. K., Bradley, R. S., Miller, S. K., Rutherford, S., et al. (2008). Proxy-based reconstructions of hemispheric and global surface temperature variations over the past two millennia. *Proc. Natl. Acad. Sci.* 105, 13252–13257. doi:10.1073/pnas.0805721105

Mann, M. E., Zhang, Z., Rutherford, S., Bradley, R. S., Hughes, M. K., Shindell, D., et al. (2009). Global signatures and dynamical origins of the Little ice age and medieval climate anomaly. *Science* 326, 1256–1260. doi:10.1126/science.1177303

Marcott, S. A., Shakun, J. D., Clark, P. U., and Mix, A. C. (2013). A reconstruction of regional and global temperature for the past 11,300 years. *Science* 339, 1198–1201. doi:10.1126/science.1228026

Margaritelli, G., Cacho, I., Català, A., Barra, M., Bellucci, L. G., Lubritto, C., et al. (2020). Persistent warm Mediterranean surface waters during the Roman period. *Sci. Rep.* 10, 10431. doi:10.1038/s41598-020-67281-2

Marsicek, J., Shuman, B. N., Bartlein, P. J., Shafer, S. L., and Brewer, S. (2018). Reconciling divergent trends and millennial variations in Holocene temperatures. *Nature* 554, 92–96. doi:10.1038/nature25464

Matero, I. S. O., Gregoire, L. J., Ivanovic, R. F., Tindall, J. C., and Haywood, A. M. (2017). The 8.2 ka cooling event caused by Laurentide ice saddle collapse. *Earth Planet. Sci. Lett.* 473, 205–214. doi:10.1016/j.epsl.2017.06.011

Mauritzen, C., and Häkkinen, S. (1997). Influence of sea ice on the thermohaline circulation in the Arctic-North Atlantic Ocean. *Geophys. Res. Lett.* 24, 3257–3260. doi:10.1029/97GL03192

Max, L., Lembke-Jene, L., Riethdorf, J.-R., Tiedemann, R., Nürnberg, D., Kühn, H., et al. (2014). Pulses of enhanced North Pacific intermediate water ventilation from the okhotsk sea and bering sea during the last deglaciation. *Clim. Past.* 10, 591–605. doi:10.5194/cp-10-591-2014

Max, L., Riethdorf, J.-R., Tiedemann, R., Smirnova, M. A., Lembke-Jene, L., Fahl, K., et al. (2012). Sea surface temperature variability and sea-ice extent in the subarctic northwest Pacific during the past 15,000 years. *Paleoceanography* 27. doi:10.1029/2012PA002292

Mayewski, P. A., Meeker, L. D., Twickler, M. S., Whitlow, S., Yang, Q., Lyons, W. B., et al. (1997). Major features and forcing of high-latitude northern hemisphere atmospheric circulation using a 110,000-year-long glaciochemical series. *J. Geophys. Res. Ocean.* 102, 26345–26366. doi:10.1029/96JC03365

Mayewski, P. A., Rohling, E. J., Curt Stager, J., Karlén, W., Maasch, K. A., David Meeker, L., et al. (2004). Holocene climate variability. *Holocene Clim. Var. Quat. Res.* 62, 243–255. doi:10.1016/j.yqres.2004.07.001

McManus, J. F., Francois, R., Gherardi, J.-M., Keigwin, L. D., and Brown-Leger, S. (2004). Collapse and rapid resumption of Atlantic meridional circulation linked to deglacial climate changes. *Nature* 428, 834–837. doi:10.1038/nature02494

Meehl, G. A., Arblaster, J. M., Matthes, K., Sassi, F., and van Loon, H. (2009). Amplifying the pacific climate system response to a small 11-year solar cycle forcing. *Science* 325, 1114–1118. doi:10.1126/science.1172872

Moros, M., Andrews, J. T., Eberl, D. D., and Jansen, E. (2006). Holocene history of drift ice in the northern North Atlantic: evidence for different spatial and temporal modes. *Paleoceanography* 21, PA2017. doi:10.1029/2005PA001214

Moy, C. M., Seltzer, G. O., Rodbell, D. T., and Anderson, D. M. (2002). Variability of El niño/southern oscillation activity at millennial timescales during the holocene epoch. *Nature* 420, 162–165. doi:10.1038/nature01194

Münnich, M., Cane, M. A., and Zebiak, S. E. (1991). A study of self-excited oscillations of the tropical ocean–atmosphere system. Part II: nonlinear cases. *J. Atmos. Sci.* 48, 1238–1248. doi:10.1175/1520-0469(1991)048<1238:asoseo>2.0.co;2

Nazarova, L. B., Razjigaeva, N. G., Golovatyuk, L. V., Biskaborn, B. K., Grebennikova, T. A., Ganzey, L. A., et al. (2021). Reconstruction of environmental conditions in the eastern part of primorsky krai (Russian far east) in the late holocene. *Contemp. Probl. Ecol.* 14, 218–230. doi:10.1134/S1995425521030094

Neff, U., Burns, S. J., Mangini, A., Mudelsee, M., Fleitmann, D., and Matter, A. (2001). Strong coherence between solar variability and the monsoon in Oman between 9 and 6 kyr ago. *Nature* 411, 290–293. doi:10.1038/35077048

Olsen, J., Anderson, N. J., and Knudsen, M. F. (2012). Variability of the North Atlantic Oscillation over the past 5,200 years. *Nature Geosci.* 5, 808–812. doi:10.1038/ngeo1589

Rasmussen, S. O., Bigler, M., Blockley, S. P., Blunier, T., Buchardt, S. L., Clausen, H. B., et al. (2014). A stratigraphic framework for abrupt climatic changes during the Last Glacial period based on three synchronized Greenland ice-core records: refining and extending the INTIMATE event stratigraphy. *Quat. Sci. Rev.* 106, 14–28. doi:10.1016/j.quascirev.2014.09.007

Razjigaeva, N. G., Ganzey, L. A., Grebennikova, T. A., Mokhova, L. M., Rybin, A. V., Nazarova, L. B., et al. (2022). Environmental changes since 14 ka BP in the southernmost Kuril islands (North-Western Pacific) and regional correlation of events. *J. Asian Earth Sci.* 226, 105088. doi:10.1016/j.jseaes.2022.105088

Riethdorf, J.-R., Max, L., Nürnberg, D., Lembke-Jene, L., and Tiedemann, R. (2013a). Deglacial development of (sub) sea surface temperature and salinity in the subarctic northwest Pacific: implications for upper-ocean stratification. *Paleoceanography* 28, 91–104. doi:10.1002/palo.20014

Riethdorf, J.-R., Nürnberg, D., Max, L., Tiedemann, R., Gorbarenko, S. A., and Malakhov, M. I. (2013b). Millennial-scale variability of marine productivity and terrigenous matter supply in the western Bering Sea over the past 180 kyr. *Clim. Past.* 9, 1345–1373. doi:10.5194/cp-9-1345-2013

Sadekov, A. Y., Ganeshram, R., Pichevin, L., Berdin, R., McClymont, E., Elderfield, H., et al. (2013). Palaeoclimate reconstructions reveal a strong link between El Niño-Southern Oscillation and Tropical Pacific mean state. *Nat. Commun.* 4, 2692. doi:10.1038/ncomms3692

Scafetta, N., Milani, F., Bianchini, A., and Ortolani, S. (2016). On the astronomical origin of the Hallstatt oscillation found in radiocarbon and climate records throughout the Holocene. *Earth-Science Rev.* 162, 24–43. doi:10.1016/j.earscirev.2016.09.004

Schneider, T., Bischoff, T., and Haug, G. H. (2014). Migrations and dynamics of the intertropical convergence zone. *Nature* 513, 45–53. doi:10.1038/nature13636

Seki, O., Ikehara, M., Kawamura, K., Nakatsuka, T., Ohnishi, K., Wakatsuchi, M., et al. (2004). Reconstruction of paleoproductivity in the Sea of Okhotsk over the last 30 kyr. *Paleoceanography* 19. doi:10.1029/2002PA000808

Seki, O., Sakamoto, T., Sakai, S., Schouten, S., Hopmans, E. C., Damsté, J. S. S., et al. (2009). Large changes in seasonal sea ice distribution and productivity in the Sea of Okhotsk during the deglaciations. *Geochem. Geophys. Geosystems* 10, 1–10. doi:10.1029/2009GC002613

Shindell, D. T., Schmidt, G. A., Mann, M. E., Rind, D., and Waple, A. (2001). Solar forcing of regional climate change during the maunder minimum. *Science* 294, 2149–2152. doi:10.1126/science.1064363

Sigl, M., Toohey, M., McConnell, J. R., Cole-Dai, J., and Severi, M. (2022). Volcanic stratospheric sulfur injections and aerosol optical depth during the Holocene (past 11,500 years) from a bipolar ice core array. *Earth Syst. Sci. Data* 14, 3167–3196.

Sigl, M., Winstrup, M., McConnell, J. R., Welten, K. C., Plunkett, G., Ludlow, F., et al. (2015). Timing and climate forcing of volcanic eruptions for the past 2,500 years. *Nature* 523, 543–549. doi:10.1038/nature14565

Simonenko, S. V. (2013). Fundamentals of the thermohydrogravidynamic theory of the global seismotectonic activity of the earth. *Int. J. Geophys.* 2013, 1–39. doi:10.1155/2013/519829

Solomina, O. N., Bradley, R. S., Hodgson, D. A., Ivy-Ochs, S., Jomelli, V., Mackintosh, A. N., et al. (2015). Holocene glacier fluctuations. *Quat. Sci. Rev.* 111, 9–34. doi:10.1016/j.quascirev.2014.11.018

Solomon, S., Qin, D., and Manning, M. (2007). *IPCC, 2007: climate change 2007: the physical science basis. Contribution of working group I to the fourth assessment report of the intergovernmental panel on climate change* (Cambridge: Cambridge University Press).

Soon, W., Baliunas, S., Posmentier, E. S., and Okeke, P. (2000). Variations of solar coronal hole area and terrestrial lower tropospheric air temperature from 1979 to mid-1998: astronomical forcings of change in earth's climate? *New Astron.* 4, 563–579. doi:10.1016/s1384-1076(00)00002-6

Stager, J. C., Cumming, B., and Meeker, L. (1997). A high-resolution 11,400-yr diatom record from lake victoria, east africa. *Quat. Res.* 47, 81–89. doi:10.1006/qres.1996.1863

Steinhilber, F., Abreu, J. A., Beer, J., Brunner, I., Christl, M., Fischer, H., et al. (2012). 9,400 years of cosmic radiation and solar activity from ice cores and tree rings. *Proc. Natl. Acad. Sci.* 109, 5967–5971. doi:10.1073/pnas.1118965109

Stoner, J. S., Jennings, A., Kristjánsdóttir, G. B., Dunhill, G., Andrews, J. T., and Hardardóttir, J. (2007). A paleomagnetic approach toward refining Holocene radiocarbon-based chronologies: paleoceanographic records from the north Iceland (MD99-2269) and east Greenland (MD99-2322) margins. *Paleoceanography* 22, PA1209. doi:10.1029/2006PA001285

Sun, Q., Liu, Y., Wünnemann, B., Peng, Y., Jiang, X., Deng, L., et al. (2019). Climate as a factor for Neolithic cultural collapses approximately 4000 years BP in China. *Earth-Science Rev.* 197, 102915. doi:10.1016/j.earscirev.2019.102915

Tarasov, P. E., Savelieva, L. A., Long, T., and Leipe, C. (2019). Postglacial vegetation and climate history and traces of early human impact and agriculture in the present-day cool mixed forest zone of European Russia. *Quat. Int.* 516, 21–41. doi:10.1016/j.quaint.2018.02.029

Torrence, C., and Compo, G. P. (1998). A practical guide to wavelet analysis. *Bull. Am. Meteorol. Soc.* 79, 61–78. doi:10.1175/1520-0477(1998)079<0061:apgtwa>2.0.co;2

Tziperman, E., Zebiak, S. E., and Cane, M. A. (1997). Mechanisms of seasonal – ENSO interaction. *J. Atmos. Sci.* 54, 61–71. doi:10.1175/1520-0469(1997)054<0061:mosei>2.0.co;2

Usoskin, I. G., Gallet, Y., Lopes, F., Kovaltsov, G. A., and Hulot, G. (2016). Solar activity during the Holocene: the Hallstatt cycle and its consequence for grand minima and maxima. *Astron. Astrophys.* 587, A150. doi:10.1051/0004-6361/201527295

Usoskin, I. G., Solanki, S. K., and Kovaltsov, G. A. (2007). Grand minima and maxima of solar activity: new observational constraints. *Astron. Astrophys.* 471, 301–309. doi:10.1051/0004-6361:20077704

Wang, P. X., Wang, B., Cheng, H., Fasullo, J., Guo, Z., Kiefer, T., et al. (2017). The global monsoon across time scales: mechanisms and outstanding issues. *Earth-Science Rev.* 174, 84–121. doi:10.1016/j.earscirev.2017.07.006

Wang, Y., Cheng, H., Edwards, R. L., An, Z., Wu, J., Shen, C.-C., et al. (2001). A high-resolution absolute-dated late Pleistocene Monsoon record from Hulu Cave, China. *Science* 294, 2345–2348. doi:10.1126/science.1064618

Wang, Y., Cheng, H., Edwards, R. L., He, Y., Kong, X., An, Z., et al. (2005). The Holocene Asian monsoon: links to solar changes and North Atlantic climate. *Science* 308, 854–857. doi:10.1126/science.1106296

Wang, Y., Cheng, H., Edwards, R. L., Kong, X., Shao, X., Chen, S., et al. (2008). Millennial- and orbital-scale changes in the East Asian monsoon over the past 224,000 years. *Nature* 451, 1090–1093. doi:10.1038/nature06692

Wanner, H., Mercolli, L., Grosjean, M., and Ritz, S. P. (2015). Holocene climate variability and change; a data-based review. *J. Geol. Soc. Lond.* 172, 254–263. doi:10.1144/jgs2013-101

Wanner, H., Solomina, O., Grosjean, M., Ritz, S. P., and Jetel, M. (2011). Structure and origin of Holocene cold events. *Quat. Sci. Rev.* 30, 3109–3123. doi:10.1016/j.quascirev.2011.07.010

White, S. M., Ravelo, A. C., and Polissar, P. J. (2018). Dampened El Niño in the early and mid-holocene due to insolation-forced warming/deepening of the thermocline. *Geophys. Res. Lett.* 45, 316–326. doi:10.1002/2017GL075433

Wu, W., and Liu, T. (2004). Possible role of the "Holocene event 3" on the collapse of neolithic cultures around the central plain of China. *Quat. Int.* 117, 153–166. doi:10.1016/s1040-6182(03)00125-3

Yan, H., Wei, W., Soon, W., An, Z., Zhou, W., Liu, Z., et al. (2015). Dynamics of the intertropical convergence zone over the western pacific during the Little ice age. *Nat. Geosci.* 8, 315–320. doi:10.1038/ngeo2375

Zhang, P., Cheng, H., Edwards, R. L., Chen, F., Wang, Y., Yang, X., et al. (2008). A test of climate, Sun, and culture relationships from an 1810-year Chinese cave record. *Science* 322, 940–942. doi:10.1126/science.1163965

Zhong, Y., Miller, G. H., Otto-Bliesner, B. L., Holland, M. M., Bailey, D. A., Schneider, D. P., et al. (2011). Centennial-scale climate change from decadally-paced explosive volcanism: a coupled sea ice-ocean mechanism. *Clim. Dyn.* 37, 2373–2387. doi:10.1007/s00382-010-0967-z